coatings

MDPI

Article

The Effect of Opto-Electronic Transition Type on the Electric Resistivity of Cr-Doped Co_3O_4 Thin Films

A. M. Faramawy [1,*], Hamada Elsayed [2,3], Mohamed Sabry [4] and H. M. El-Sayed [1]

[1] Department of Physics, Faculty of Science, Ain Shams University, Abbassia, Cairo 11566, Egypt
[2] Department of Industrial Engineering, Università Degli Studi di Padova, 35131 Padova, Italy
[3] Refractories, Ceramics and Building Materials Department, National Research Centre, Cairo 12622, Egypt
[4] Physics Department, College of Applied Sciences, Umm Al-Qura University, Mecca 24382, Saudi Arabia
* Correspondence: ahmed_faramawy@sci.asu.edu.eg

Abstract: Cr-doped Co_3O_4 thin films were prepared by spray pyrolysis on soda-lima glass. The structure and morphology of the prepared samples were characterized by grazing incidence X-ray diffraction (GIXRD), Fourier-transform infrared spectroscopy (FTIR) and Scanning electron Microscopy (SEM). The results indicated the formation of a single cubic spinel phase with a crystallite size of about 6 nm. Different electronic transitions and estimations of the band gap structure were determined from the optical absorption spectra. The dependence of electrical resistivity on Cr content was investigated. It was found that the resistivity increased by increasing the Cr content. In addition, the effect of photon excitation on the electrical properties showed that the electrical resistivity decreased under visible illumination ($\lambda_{vis.}$ = 532 nm) and increased under infrared illumination (λ_{IR} = 780 nm). The relative change in resistivity (sensitivity) under both light illuminations was enhanced by increasing the Cr content. Therefore, this work introduces a new application for Co_3O_4 material as a light detector.

Keywords: Cr-doped Co_3O_4; thin film; spray pyrolysis; optical and electrical properties

Citation: Faramawy, A.M.; Elsayed, H.; Sabry, M.; El-Sayed, H.M. The Effect of Opto-Electronic Transition Type on the Electric Resistivity of Cr-Doped Co_3O_4 Thin Films. *Coatings* **2023**, *13*, 328. https://doi.org/10.3390/coatings13020328

Academic Editor: Ajay Vikram Singh

Received: 12 January 2023
Revised: 23 January 2023
Accepted: 30 January 2023
Published: 1 February 2023

1. Introduction

Thin film materials introduce unique physical and chemical properties in comparison to bulk ones. These properties arise mainly from quantum confinement effects and the increase of the surface atoms decreasing the particle size [1–3]. Transition metal oxide thin films have attracted physical properties, such as their chemical stability, tunning their electric and optical properties [4–7]. Cobalt oxide is known as a promising material due to its applications in many fields, such as CO gas sensors [8], solar absorbers at high temperatures [9], photocatalysts for dye degradation in water purification, and magnetic materials [10]. In the form of thin films, cobalt oxide is used as an electrode in super capacitor design and in the fabrication of electrochromic devices [11] as a result of changing its optical properties under an external electrical stimulus [12]. Enhancing the different properties of Co_3O_4 could be obtained by changing the method of preparation to control particle size and morphology [13] or by making substitutional doping with other transition elements [14,15]. The effect of doping on the different properties of Co_3O_4 arises from the ionic radius, electronic structure and the cation distribution of the dopant ions. Therefore, monitoring of the physical properties could be obtained by changing the type of dopant in addition to its concentration. Furthermore, the method of preparation for Co_3O_4 thin film has great effects on the magnetic, electric and optical properties of the prepared samples. These effects are attributed to the change in the crystallite size, morphology and texture of the prepared samples [10–12]. In particular, many techniques have been reported for the synthesis of Co_3O_4 thin films, such as chemical vapor deposition [13,14] and chemical spray pyrolysis [16]. Owing to their simplicity and inexpensiveness, chemical spray pyrolysis techniques have been used to prepare thin films.

Cr-doping has considerable effects on the different properties of Co_3O_4, especially on their optical absorption in the visible region [9]. In addition, the optical properties of Co_3O_4 could be changed under the effect of an external electrical signal [14].

In the present work, the change in the electrical properties under the effect of photon irradiation in both visible and near infrared regions at different concentrations of Cr doping will be investigated.

2. Materials and Methods

Chemical spray pyrolysis was used to deposit cobalt oxide and chromium-doped cobalt oxide thin films ($Cr_xCo_{3-x}O_4$) on properly cleaned soda lime glass substrates. High-purity Cr-nitrates ($Cr(NO_3)_3 \cdot 9H_2O$) (99.9%, LOBAChemie) and Co-nitrates ($Co(NO_3)_2 \cdot 6H_2O$) (98%, Merk, India) were dissolved in a solution of distilled water and ethanol at a ratio of 1:3, creating the precursor solution. A two-directional motorized micro nozzle with air as a carrier gas was used. The growth time was kept constant for all sprayed films (20 s) and the optimal substrate temperature for synthesizing $Cr_xCo_{3-x}O_4$ thin films of good quality was found to be 400 $\pm$ 10 °C. Furthermore, grazing incidence X-ray diffraction (GIXRD) (Philips X'Pert PRO MRD triple axis diffractometer (angular resolution 0.01°, precision 0.001°)) was used to obtain the cubic phase structure of the samples. The crystal structure of the $Cr_xCo_{3-x}O_4$ was refined using the Rietveld profile method, using MAUD software [17]. Fourier transform infrared spectroscopy (FTIR) was performed at room temperature in transmission mode (Shimadzu, Qatr-S single reflection ATR, Kyoto, Japan) in the range of 400–4000 cm^{-1}. A scanning electron microscope (SEM) (Zeiss Field-emission SEM (FE-SEM), Jena, Germany) was used to determine the surface morphology. The optical properties of the films were measured using a UV-Vis optical spectroscopy (Jasco Ltd. V-670 UV-Vis-NIR, Heckmondwike, UK) spectrophotometer with a working range of 200–800 nm. In order to study the photo-resistance behavior of the investigated films, a two probe method with a KEITHLEY 6514 system electrometer was used in dark and under illumination of both infra-red and visible light sources.

3. Results

3.1. X-ray Analysis

Figure 1I depicts the grazing incident X-ray diffractograms (GIXRD) of Co_3O_4 and Cr^{3+} doped Co_3O_4 thin film samples with varying concentrations (x = 0.02, 0.04, 0.06, 0.08 and 0.1). Consistent with ICSD card 28058 [18] and JCPDS No. 24-0326 [19], a single cubic structure phase of Co_3O_4 and $Cr_xCo_{3-x}O_4$ thin films, respectively, was obtained from diffraction peaks at (220), (311), (400), (511), and (440). GIXRD measurements show that the undoped and Cr^{3+} doped Co_3O_4 thin films form in a spinel structure system with a cubic lattice structure (space group: $O_m^7 - Fd3m$) [20]. However, Figure 1II reveals that effective incorporation of Cr^{3+} dopant in the Co_3O_4 host matrix causes a shift of the prominent peak of the crystal planes (311) toward the lower diffraction angles, which in turn means a decrease in inter planar distances. This could be explained by the larger ionic radius of Cr^{3+} (0.63 Å) [10] compared to that of Co^{3+} (0.53 Å) [19]. This proves that the Cr^{3+} ion substitutes for the positions of Co^{3+} ions in the structure.

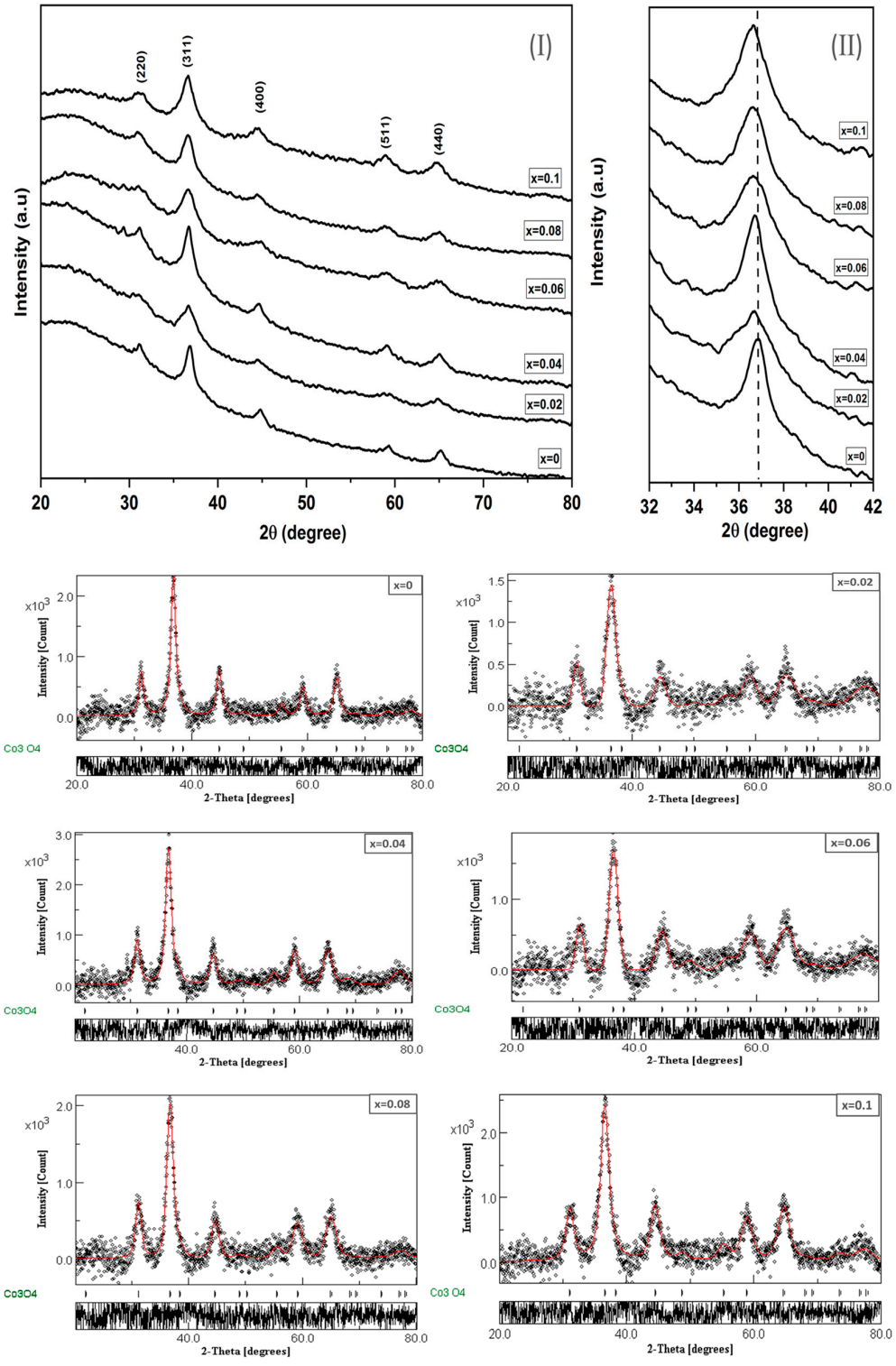

Figure 1. (**I**) XRD patterns of Cr doped Co_3O_4 (**II**) the shifting of (311) peaks positions to lower 2θ values and Rietveld refinement profile for $Cr_xCo_{3-x}O_4$ thin films using MAUD program.

Furthermore, to examine the crystal structural phase and to obtain the lattice constants, all investigated samples were examined for Rietveld analysis using the MAUD software program [21], and the fitted profile results for all investigated thin films are shown in Figure 1. In addition, the refinement cycle was repeated until convergence with a goodness factor near one was attained [10].

The lattice constant (a) of all prepared $Cr_xCo_{3-x}O_4$ thin films was evaluated from the fitted data and is listed in Table 1. The theoretical density $D_{x\text{-ray}}$ is calculated from:

$$D_{x\text{-ray}} = \frac{ZM}{V\,N_A}$$

where Z is the number of molecules per unit cell (Z = 8), M is the molecular weight of the undoped and doped spinel cobalt, V is the volume of the unit cell and N_A is Avogadro's number. Table 1 shows that the $D_{x\text{-ray}}$ decreased with the addition of Cr^{3+} content. This can be attributed to the substitution of Cr^{3+} ions (51.996 amu) by heavier Co^{2+} ions (58.933 amu) [10]. Moreover, the micro strain and the average crystallite size are determined from the Williamson–Hall (W-H) equation [22]. Table 1 depicts the change in strain (ε) and average crystallite size (R) with the Cr^{3+} content. It is obvious that the crystallite size decreases with increasing the Cr^{3+} content while the strain has inverse behavior. This could be understood in terms of the difference in the ionic radii of Co^{3+} and Cr^{3+}, where the presence of Cr^{3+}, which has a larger ionic radius, causes more stress on the unit cell. This reflects the increase of the macrostrain with increasing the Cr content. Moreover, the increase in the macrostrain increases the lattice imperfection, which prevents crystal growth and thus decreases the crystallite size. For more confirmation about the defects in the prepared films, the dislocation density (δ), the length of dislocation lines per crystal lattice unit volume, is calculated from equation [23] $\delta = \frac{1}{R^2}$, where R is the crystallite size.

Table 1. Lattice parameter (a), cell volume (V), crystallite size (R), strain (ε) and dislocation density (δ), for $Cr_xCo_{3-x}O_4$ thin film samples.

Cr Content (x)	0	0.02	0.04	0.06	0.08	0.1
a (Å)	8.087	8.113	8.117	8.123	8.128	8.130
V (Å^3)	528.97	533.9	534.8	536.11	536.97	537.38
R (nm)	8.2	4.5	6.9	4.5	5.7	5.3
$D_{x\text{-ray}}$ (g cm^{-3})	6.047	5.987	5.974	5.953	5.943	5.935
ε × 10^{-3}	3.50	2.70	9.70	11.4	16.7	22.5
δ × 10^{-3} (nm^{-2})	15.2	50.1	20.9	15.2	30.1	34.4

It is clear from Table 1 that the obtained dislocation density is significantly increased with increasing Cr^{3+} content which infers that dopant atoms occupy substitutional positions in the matrix. The variation in δ and strain in the investigated films confirms the presence of defects in the lattice structure due to the contribution of the Cr^{3+} ions that cause changes in different physical properties.

3.2. FTIR Analysis

To study the cation distribution, the FTIR spectra for all investigated samples are shown in Figure 2. It is obvious that there are two main bands around 558 cm^{-1} and 650 cm^{-1}. The first one is assigned to the LO vibrational mode of Co^{2+} ions in the tetrahedral environment of oxygen ions (Co^{2+}–O) while the band above 650 cm^{-1} corresponds to the longitudinal optical vibrations (LO) of Co^{3+} in the octahedral site of the spinel, which is related to (Co^{3+}–O) bond [24,25]. Furthermore, the dopant samples exhibit a small shift in the octahedral site band to a higher value, which confirms the presence of the Cr^{3+} ions in the octahedral site. The appearance of the band around 834 cm^{-1} is attributed to one of the vibrational modes of the nitrate group of the precursors [26]. The study of the FTIR spectrum confirms that Co^{2+} ions occupy the tetrahedral sites (A site) while, both Co^{3+} and Cr^{3+} ions occupy the octahedral sites (B site), i.e., the proposed cation distribution is $[Co^{2+}]_A.O.(Co^{3+}{}_{(1-x)}Cr^{3+}{}_x)_B$.

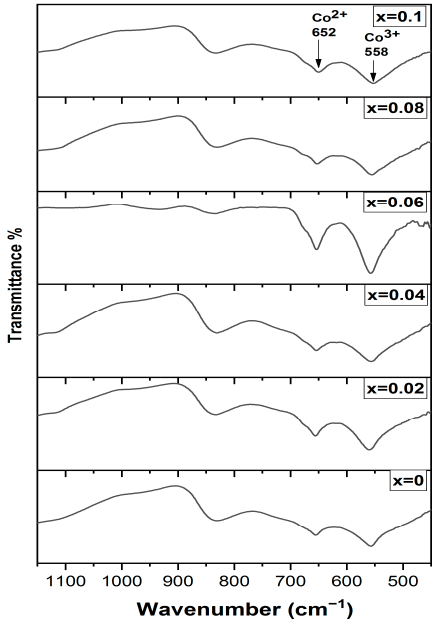

Figure 2. FTIR spectra of Cr doped Co_3O_4 thin films.

3.3. Scanning Electron Microscope (SEM)

Figure 3 depicts the scanning electron microscope images for x = 0.0, 0.02, 0.06 and 0.1 of $Cr_xCo_{3-x}O_4$ thin films. One can see that the surface image of the samples is homogeneous and smooth. It is also observed that the un-doped cobalt spinel film shows a granular surface, which disappeared in Cr^{3+} doped films due to the decrease of the crystallite size, as mentioned in the X-ray study.

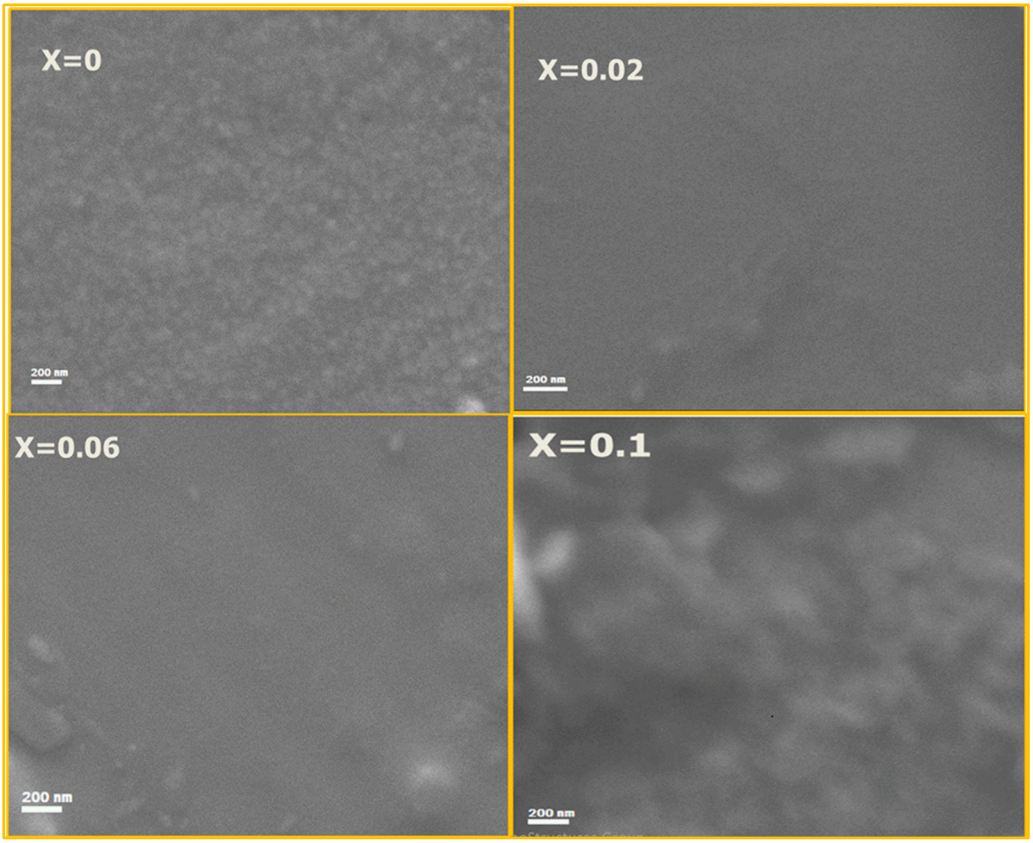

Figure 3. SEM images of x = 0.00, 0.02, 0.04 and 0.1 of Cr doped Co_3O_4 thin films.

3.4. Optical Properties and Band Gap

It is known that optical properties strongly depend on the electronic structure, which in turn is affected by the dopant elements. The absorption spectra for the investigated samples, in the wavelength range from 350 to 2700 nm, are given in Figure 4I. It is obvious that for pure Co_3O_4 (x = 0.0), there are three main absorption bands. To obtain the precise locations of these bands, a relation between the derivative of the absorption coefficient with respect to the photon energy is shown in Figure 4II. The first sharp transition is at 0.77 eV. This band is attributed to the charge transfer transition between d(2g) Co^{3+} in the octahedral site to d(t_2) Co^{2+} in the tetrahedral site. This mechanism is called the internal oxidation process. The 2nd band is located at 1.56 eV. This band originates from the charge transfer transition between P(O^{-2}) and d(e_g Co^{3+}). Finally, the 3rd transition at 2.38 eV is obtained because of the charge transfer P(O^{-2}) to d(t_2 Co^{2+}) [27–30]. Furthermore, there is a small transition beside E_{g1} band (around 0.9 eV) and the intensity of this band decreases by increasing Cr content. This transition is attributed to the excitation of the small hopping polaron formed between Co^{3+} and Co^{2+} [31]. Moreover, the width of the 2nd band (E_{g2}) increases from the red side of the band by increasing Cr^{3+} content. The effects of Cr doping on the positions of the absorption bands are listed in Table 2. One can observe that the positions of the three bands have no considerable variations with increasing Cr content (x). The only observed change is the effect of Cr^{3+} on the width of the 2nd band transition. From the above observations, one may conclude that the presence of Cr^{3+} ions in the B-site causes the presence of new states in the d(e_g) level of Co^{3+}. As the presence of Cr^{3+} ions in the octahedral site impedes the internal oxidation between Co^{3+} and Co^{2+}, the intensity of the absorption of the corresponding band relative to the undoped sample decreases.

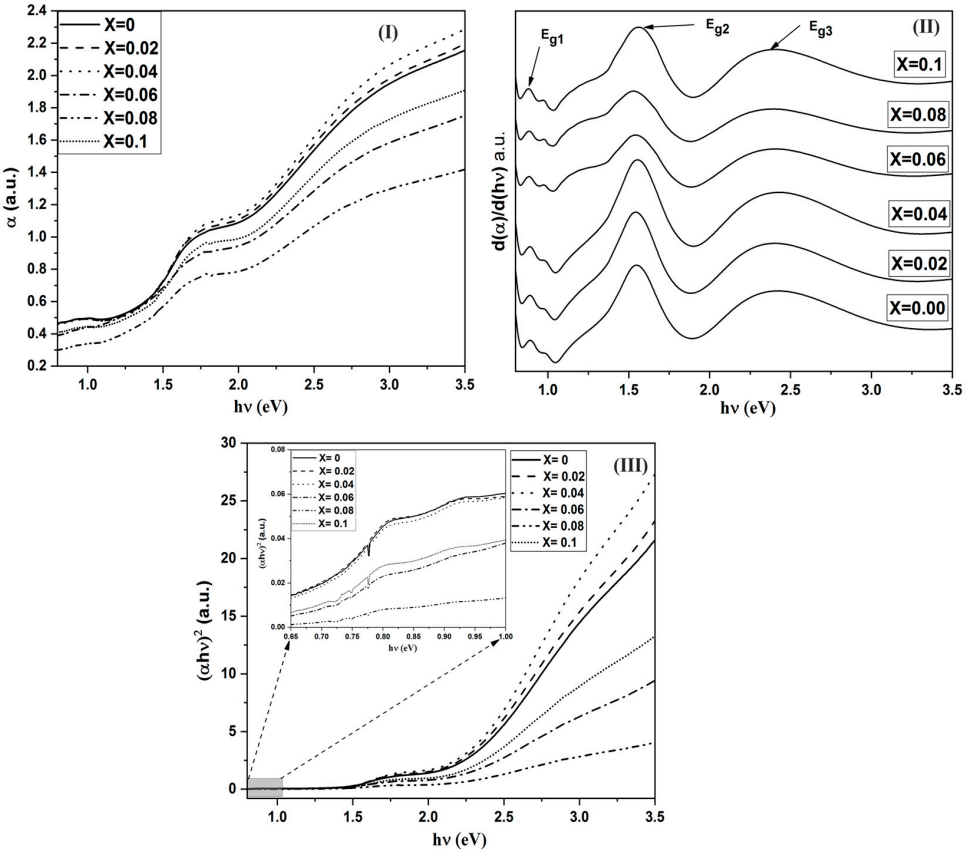

Figure 4. (**I**) the absorption coefficient against the photon energy for all films of $Cr_xCo_{3-x}O$, (**II**) the derivative of α against the photon energy for $Cr_xCo_{3-x}O_4$ samples and (**III**) the variation of $(\alpha h\nu)^2$ against the photon energy for all films of $Cr_xCo_{3-x}O_4$.

Table 2. The energy band gaps (E_{g1}, E_{g2} and E_{g3}) obtained from Tauc and derivative relations, hopping lengths and sub-sites radii for $Cr_xCo_{3-x}O_4$ thin film samples.

	Eg_1 (eV)		Eg_2 (eV)		Eg_3 (eV)	
X	**Derivative**	**Tauc**	**Derivative**	**Tauc**	**Derivative**	**Tauc**
0	0.79	0.80	1.55	1.46	2.42	2.22
0.02	0.79	0.82	1.54	1.46	2.42	2.22
0.04	0.79	0.82	1.55	1.47	2.42	2.211
0.06	0.78	0.80	1.54	1.44	2.42	2.19
0.08	0.78	0.81	1.53	1.45	2.40	2.18
0.1	0.78	0.82	1.55	1.47	2.41	2.21

To obtain the type of the three band transitions, the Tauc & Davis–Mott relation is used, where according to this relation [32,33]:

$$\alpha h\nu = A(h\nu - E_g)^n$$

The value of n determines the type of electronic transition or optical transition. If $n = 1/2$ then the transition is a direct allowed transition, $n = 2$ indirect allowed transition, $n = 3/2$ direct forbidden transition, and $n = 3$ is the indirect forbidden energy [34]. The plot of $(\alpha h\nu)^2$ vs. the photon energy ($h\nu$), as shown in Figure 4III, exhibiting acute absorption boundary and E_g was calculated by fitting the linear part of each region. By comparing the values of the energy gaps obtained from Tauc's relation and the differentiation method, there is a good match between the two methods. The difference arises from the linear fitting of Tauc's method. Therefore, we may assume that the derivative method is more accurate. Hence, we can conclude that the electronic transitions belong to the direct allowed type. Furthermore, the sum of E_{g1} and E_{g2} is almost equal to E_{g3}. This means that the $d(e_g)$ level of Co^{3+} lies in the energy gap between the valance band of $P(O^{-2})$ and the conduction band of $d(t_2)$ of Co^{2+} in tetrahedral sites. The proposed energy band diagram is shown in Figure 5.

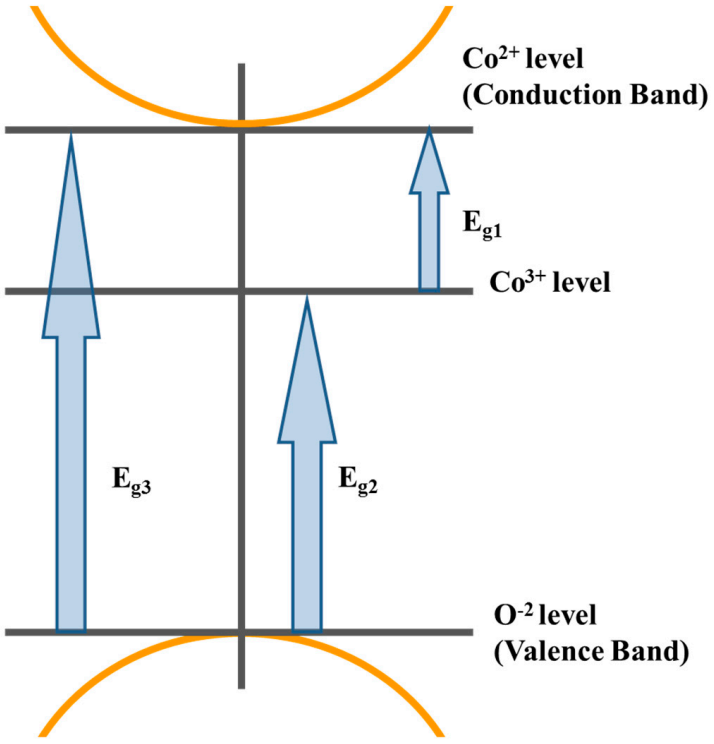

Figure 5. The proposed schematic diagram for the optical energy bands of spinel cobalt oxide.

3.5. Photo-Resistance Measurements

The dependence of room temperature resistivity (dark measurement) on Cr content is shown in Figure 6. It is obvious that, as the Cr content increases, the resistivity increases. This could be explained in light of two factors:

1. The conduction mechanism in Co_3O_4 is due to the formation of a small polaron hopping between Co^{3+} and Co^{2+}. As the Co^{3+} in the octahedral site is substituted by Cr^{3+} then the amount of Co^{3+} decreases and so the hopping between Co^{3+} and Co^{2+} decreases and subsequently, the resistivity increases.
2. As the ionic radius of Cr^{3+} is greater than the radius Co^{3+} then the rate of hopping will be lower because of the large distance between the ions and this in turn will increase the resistivity.

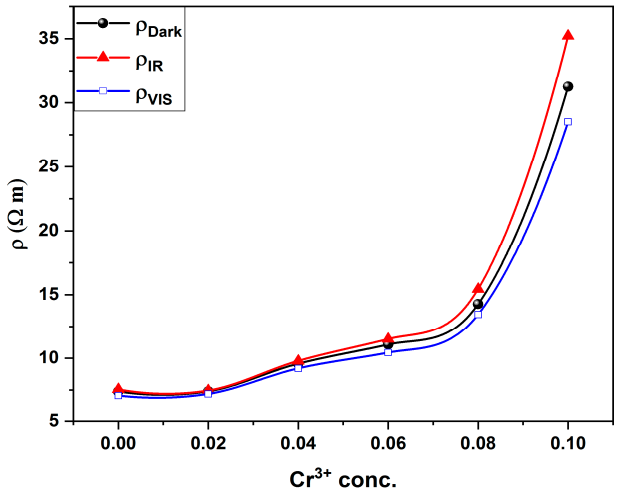

Figure 6. Resistivity of (dark, IR and Vis) against Cr^{3+} concentration for all investigated thin films.

To study the effect of the electronic transition on the electrical resistivity of the investigated samples, two excitation wavelengths are used. One of them matches the E_{g2} transition (1.56 eV or λ_{ir} = 780 nm) and the other for E_{g3} transition (2.38 eV or λ_{vis} = 532 nm). LED's at the proper wavelengths are used as a source of excitation. Figure 6 shows the variation in electric resistivity under the illumination of both excitation wavelengths. It is valuable to mention that the resistivity of the samples increases under illumination by λ_{ir} while it decreases under illumination by $\lambda_{vis.}$ Additionally, as shown in Figure 7, the relative change in resistivity increases with increasing Cr content (x) for both wavelengths.

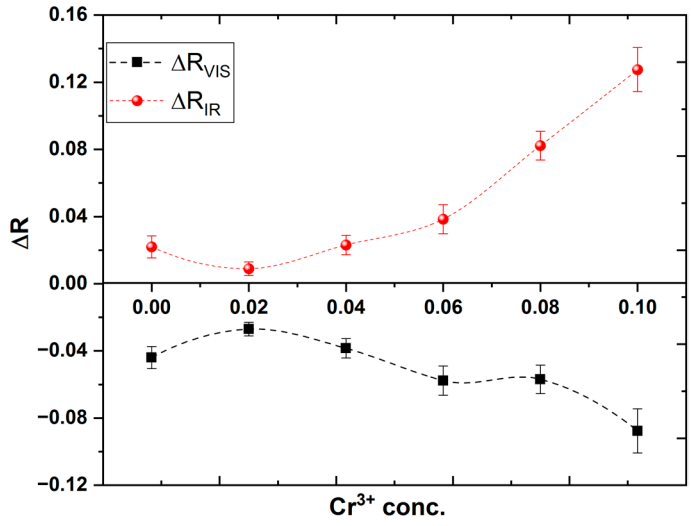

Figure 7. Relative change in resistivity against Cr^{3+} concentration for all investigated thin films.

The decrease in resistivity under the illumination of $\lambda_{vis.}$ could be understood in terms of the generation of electron-hole pairs in the valance and conduction bands, as mentioned in the 3rd band transition from the absorption spectrum. While λ_{ir} could transfer the electrons from the valance band to the level of d(e_g) of Co^{3+} in the octahedral site, which lies in the energy gap. The trapping of the exciting electrons in the d(e_g) level will change the valance state of some Co^{3+} ions into Co^{2+} which in turn decreases the hopping between Co^{3+} in octahedral sites and Co^{2+} in the tetrahedral sites, which results in the decrease of the resistivity under the illumination of this wavelength.

4. Conclusions

A single cubic spinel phase of Cr-doped Co_3O_4 thin films has been prepared by the spray pyrolysis technique. From the optical absorption spectrum, the main three electronic transitions are attributed to the transition between Co^{3+} to Co^{2+}, the transition from the valance band to Co^{3+} and the 3rd one from the transition from the valance to the conduction band. The electrical resistivity increases by increasing the Cr content, which is explained in terms of the increase of the lattice parameter and the decrease of Co content in the samples. The electrical resistivity was found to decrease under visible illumination ($\lambda_{vis.}$ = 532 nm), while it increased under infrared illumination (λ_{IR} = 780 nm). Sensitivity under light illumination was enhanced by increasing the Cr content. This study introduces the samples as photocatalyst materials under visible illumination and as photodetectors for the near IR region.

Author Contributions: Conceptualization, A.M.F. and H.M.E.-S.; Data curation, A.M.F., H.E., M.S. and H.M.E.-S.; Formal analysis, A.M.F. and H.M.E.-S.; Funding acquisition, M.S. and H.M.E.-S.; Investigation, A.M.F. and H.M.E.-S.; Methodology, A.M.F. and H.M.E.-S.; Resources, M.S.; Validation, A.M.F., H.E., M.S. and H.M.E.-S.; Visualization, A.M.F., H.E., M.S. and H.M.E.-S.; Writing—original draft, A.M.F., M.S. and H.M.E.-S.; Writing—review & editing, A.M.F., H.E., M.S. and H.M.E.-S. All authors have read and agreed to the published version of the manuscript.

Funding: This research was funded by The Deanship Scientific Research at Umm Al-Qura University, grant number (22UQU4320621DSR01).

Institutional Review Board Statement: Not applicable.

Data Availability Statement: Not applicable.

Acknowledgments: The authors would like to thank the Deanship of Scientific Research at Umm Al-Qura University for supporting this work.

Conflicts of Interest: The authors declare no conflict of interest.

References

1. Siegel, R.W. Cluster-Assembled Nanophase Materials. *Annu. Rev. Mater. Sci.* **1991**, *21*, 559–578. [CrossRef]
2. Kodama, R.H. Magnetic Nanoparticles. *J. Magn. Magn. Mater.* **1999**, *200*, 359–372. [CrossRef]
3. Gleiter, H.H. Gleiter (1989). *Prog. Mater. Sci* **1989**, *33*, 323.
4. Cheng, C.-S.; Serizawa, M.; Sakata, H.; Hirayama, T. Electrical Conductivity of Co_3O_4 Films Prepared by Chemical Vapour Deposition. *Mater. Chem. Phys.* **1998**, *53*, 225–230. [CrossRef]
5. Raveau, B. Transition Metal Oxides: Promising Functional Materials. *J. Eur. Ceram. Soc.* **2005**, *25*, 1965–1969. [CrossRef]
6. Makhlouf, S.A.; Bakr, Z.H.; Al-Attar, H.; Moustafa, M.S. Structural, Morphological and Electrical Properties of Cr_2O_3 Nanoparticles. *Mater. Sci. Eng. B* **2013**, *178*, 337–343. [CrossRef]
7. Fouad, O.A.; El-Shall, M.S. Microwave Irradiation Assisted Growth of Cu, Ni, Co Metals And/or Oxides Nanoclusters and Their Catalytic Performance. *Nano Brief. Rep. Rev.* **2012**, *7*, 1250034. [CrossRef]
8. Yamaura, H.; Tamaki, J.; Moriya, K.; Miura, N.; Yamazoe, N. Highly Selective CO Sensor Using Indium Oxide Doubly Promoted by Cobalt Oxide and Gold. *J. Electrochem. Soc.* **1997**, *144*, L158. [CrossRef]
9. Chidambaram, K.; Malhotra, L.K.; Chopra, K.L. Spray-Pyrolysed Cobalt Black as a High Temperature Selective Absorber. *Thin Solid Films* **1982**, *87*, 365–371. [CrossRef]
10. Faramawy, A.M.; Mattei, G.; Scian, C.; Elsayed, H.; Ismail, M.I.M. Cr3+substituted Aluminum Cobalt Ferrite Nanoparticles: Influence of Cation Distribution on Structural and Magnetic Properties. *Phys. Scr.* **2021**, *96*, 125849. [CrossRef]

11. Maruyama, T.; Arai, S. Electrochromic Properties of Cobalt Oxide Thin Films Prepared by Chemical Vapor Deposition. *J. Electrochem. Soc.* **1996**, *143*, 1383. [CrossRef]
12. Granqvist, C.G. *Handbook of Inorganic Electrochromic Materials*; Elsevier: Amsterdam, The Netherlands, 1995; ISBN 008053290X.
13. Makhlouf, S.A.; Bakr, Z.H.; Aly, K.I.; Moustafa, M.S. Structural, Electrical and Optical Properties of Co_3O_4 Nanoparticles. *Superlattices Microstruct.* **2013**, *64*, 107–117. [CrossRef]
14. Zhang, Y.; Chen, Y.; Wang, T.; Zhou, J.; Zhao, Y. Synthesis and Magnetic Properties of Nanoporous Co_3O_4 Nanoflowers. *Microporous Mesoporous Mater.* **2008**, *114*, 257–261. [CrossRef]
15. Reena, R.S.; Aslinjensipriya, A.; Jose, M.; Das, S.J. Investigation on Structural, Optical and Electrical Nature of Pure and Cr-Incorporated Cobalt Oxide Nanoparticles Prepared via Co-Precipitation Method for Photocatalytic Activity of Methylene Blue Dye. *J. Mater. Sci. Mater. Electron.* **2020**, *31*, 22057–22074. [CrossRef]
16. Singh, R.N.; Koenig, J.; Poillerat, G.; Chartier, P. Electrochemical Studies on Protective Thin Co_3O_4 and $NiCo_2O_4$ Films Prepared on Titanium by Spray Pyrolysis for Oxygen Evolution. *J. Electrochem. Soc.* **1990**, *137*, 1408. [CrossRef]
17. Matthies, S.; Lutterotti, L.; Wenk, H.R. Advances in Texture Analysis from Diffraction Spectra. *J. Appl. Crystallogr.* **1997**, *30*, 31–42. [CrossRef]
18. Kalinic, B.; Girardi, L.; Ragonese, P.; Faramawy, A.; Mattei, G.; Frasconi, M.; Baretta, R.; Bogialli, S.; Roverso, M.; Rizzi, G.A.; et al. Diffusion-Driven Formation of Co_3O_4 Nanopetals Layers for Photoelectrochemical Degradation of Organophosphate Pesticides. *Appl. Surf. Sci.* **2022**, *596*, 153552. [CrossRef]
19. Liao, W.M.; Zhao, P.P.; Cen, B.H.; Jia, A.P.; Lu, J.Q.; Luo, M.F. Co–Cr–O Mixed Oxides for Low–temperature Total Oxidation of Propane: Structural Effects, Kinetics, and Spectroscopic Investigation. *Chin. J. Catal.* **2020**, *41*, 442–453. [CrossRef]
20. Roth, W.L. The Magnetic Structure of Co_3O_4. *J. Phys. Chem. Solids* **1964**, *25*, 1–10. [CrossRef]
21. Lutterotti, L.; Gualtieri, A.; Aldrighetti, S. Rietveld Refinement Using Debye-Scherrer Film Techniques. *Mater. Sci. Forum* **1996**, *228–231*, 29–34. [CrossRef]
22. Williamson, G.; Hall, W. X-ray Line Broadening from Filed Aluminium and Wolfram. *Acta Metall.* **1953**, *1*, 22–31. [CrossRef]
23. Amer, M.A.; Meaz, T.M.; Attalah, S.S.; Ghoneim, A.I. Annealing Effect on Structural Phase Transition of as-Synthesized $Mg_{0.1}Sr_{0.1}Mn_{0.8}Fe_2O_4$ Nanoparticles. *J. Alloys Compd.* **2016**, *654*, 45–55. [CrossRef]
24. Kaviyarasu, K.; Raja, A.; Devarajan, P.A. Structural Elucidation and Spectral Characterizations of Co_3O_4 Nanoflakes. *Spectrochim. Acta Part A Mol. Biomol. Spectrosc.* **2013**, *114*, 586–591. [CrossRef]
25. Tang, C.W.; Wang, C.B.; Chien, S.H. Characterization of Cobalt Oxides Studied by FT-IR, Raman, TPR and TG-MS. *Thermochim. Acta* **2008**, *473*, 68–73. [CrossRef]
26. Roy, M.; Ghosh, S.; Naskar, M.K. Solvothermal Synthesis of Cr_2O_3 Nanocubes via Template-Free Route. *Mater. Chem. Phys.* **2015**, *159*, 101–106. [CrossRef]
27. Hitkari, G.; Sandhya, S.; Gajanan, P.; Shrivash, M.K.; Deepak, K. Synthesis of Chromium Doped Cobalt Oxide (Cr: Co_3O_4) Nanoparticles by Co-Precipitation Method and Enhanced Photocatalytic Properties in the Visible Region. *J. Mater. Sci. Eng* **2018**, *7*, 2169–2222.
28. Pal, J.; Chauhan, P. Study of Physical Properties of Cobalt Oxide (Co_3O_4) Nanocrystals. *Mater. Charact.* **2010**, *61*, 575–579. [CrossRef]
29. Jacobs, J.-P.; Maltha, A.; Reintjes, J.G.H.; Drimal, J.; Ponec, V.; Brongersma, H.H. The Surface of Catalytically Active Spinels. *J. Catal.* **1994**, *147*, 294–300. [CrossRef]
30. Shelef, M.; Wheeler, M.A.Z.; Yao, H.C. Ion Scattering Spectra from Spinel Surfaces. *Surf. Sci.* **1975**, *47*, 697–703. [CrossRef]
31. Smart, T.; Pham, T.A.; Ping, Y.; Ogitsu, T. The Nature of Band Gap of Co_3O_4-a Revisit from First-Principles. *APS March Meet. Abstr.* **2019**, *2019*, C11.006.
32. Tauc, J.; Grigorovici, R.; Vancu, A. Optical Properties and Electronic Structure of Amorphous Germanium. *Phys. Status Solidi (b)* **1966**, *15*, 627–637. [CrossRef]
33. Mott, N.F.; Davis, E.A. Conduction in Non-Crystalline Systems V. Conductivity, Optical Absorption and Photoconductivity in Amorphous Semiconductors. *Philos. Mag.* **1970**, *22*, 903–922.
34. Louardi, A.; Rmili, A.; Ouachtari, F.; Bouaoud, A.; Elidrissi, B.; Erguig, H. Characterization of Cobalt Oxide Thin Films Prepared by a Facile Spray Pyrolysis Technique Using Perfume Atomizer. *J. Alloys Compd.* **2011**, *509*, 9183–9189. [CrossRef]